Reentrant quantum criticality in Yb_{2}Pd_{2}Sn

T. Muramatsu, T. Kanemasa, T. Kagayama, K. Shimizu, Y. Aoki, H. Sato, M. Giovannini, P. Bonville, V. Zlatic, I. Aviani, R. Khasanov, C. Rusu, A. Amato, K. Mydeen, M. Nicklas, H. Michor, and E. Bauer

Phys. Rev. B **83**, 180404 — Published 2 May 2011

DOI: 10.1103/PhysRevB.83.180404

Re-entrant quantum criticality in Yb_2Pd_2Sn

T. Muramatsu,[1] T. Kanemasa,[1] T. Kagayama,[1] K. Shimizu,[1] Y. Aoki,[2] H. Sato,[2] M. Giovannini,[3] P. Bonville,[4] V. Zlatic,[5] I. Aviani,[5] R. Khasanov,[6] C. Rusu,[6] A. Amato,[6] K. Mydeen,[7] M. Nicklas,[7] H. Michor,[8] and E. Bauer[8]

[1]*Kyokugen, Osaka University, Toyonaka, Osaka 560-8531, Japan*
[2]*Department of Physics, Tokyo Metropolitan University, Tokyo 192-0397, Japan*
[3]*CNR-SPIN, Dipartimento di Chimica e Chimica Industriale, University of Genova, I-16146 Genova*
[4]*CEA, Centre de Saclay, DSM/IRAMIS/SPEC 91191 Gif-sur-Yvette, France*
[5]*Instiute of Physics, Zagreb, Croatia*
[6]*Laboratory for Muon-Spin Spectroscopy, PSI, CH-5232 Villigen PSI, Switzerland*
[7]*Max Planck Institute for Chemical Physics of Solids, D-01187 Dresden, Germany*
[8]*Institute of Solid State Physics, Vienna University of Technology, A-1040 Wien, Austria*

(Dated: March 24, 2011)

We report the discovery of *two* consecutive, pressure driven magnetic instablities in Yb_2Pd_2Sn. They emerge in a non-Fermi liquid environment at the initial and the final point of a dome-like, single magnetic phase at pressures $p_{c1} \approx 1$ GPa and $p_{c2} \approx 4$ GPa. This singular behavior of Yb compounds is supposed to result from mutually competing, pressure modified energy scales, which in case of Yb_2Pd_2Sn cause a sign change of the pressure dependence of the Kondo temperature T_K and magnetic ordering temperature T_N.

PACS numbers: 71.27.+a, 71.20.Lp.72.15.Qm

In many intermetallics with Ce and Yb ions, the exchange interaction between conduction (c) electrons and f-electrons can be tuned by pressure or doping. The ensuing change in the relative weight of the RKKY and the Kondo coupling gives rise to many remarkable phenomena, like a zero-temperature quantum phase transition [1, 2] or multiple phase transitions discussed here. Ce and Yb intermetallics are often considered as electron-hole analogues, because Ce fluctuates between the $4f^1$ and $4f^0$ electronic configuration (EC), while Yb swings between the $4f^{14}$ and $4f^{13}$ state. But despite similarities, pressure experiments show that Ce and Yb intermetallics are not simply related by an electron-hole transformation. In Ce systems, pressure favors the low-volume non-magnetic $4f^0$ EC by increasing the overlap V_{fc} between the $4f$ and c wave functions. This increases the Kondo temperature, T_K, which depends exponentially on the dimensionless coupling constant $g = \Gamma/\pi|E_f|$, where $\Gamma \propto V_{fc}^2$ and E_f is the excitation energy between the magnetic and non-magnetic EC. Large values of V_{fc} can remove the crystal electric field (CEF) excitations, restore the degeneracy of the $4f$ states, and increases T_K dramatically. At large enough pressure, Ce intermetallics are always non-magnetic. In Yb systems, low-pressure favors the magnetic $4f^{13}$ EC by increasing E_f; the small size of $4f$ ions and their propensity to valence fluctuations (VF) ensures that V_{fc} does not change. Pressure, initially, reduces T_K and can lead to a magnetic ground state (GS). Once the $4f^{13}$ EC is stabilized, a further application of pressure increases V_{fc} and T_K and drives Yb intermetallics towards the VF state. In this study, we provide the first example of a Yb-based material, Yb_2Pd_2Sn, which is driven by pressure through two consecutive magnetic instabilities. The system evolves, first, from a non-magnetic to a magnetic state and, then, back to a non-magnetic one. The ensuing dome-like magnetic phase diagram has no analogy in Ce systems.

At ambient pressure, Yb_2Pd_2Sn is in a VF state, with Yb valence $\nu \approx 2.9$ [3]. In such a system, magnetic instabilities are unlikely [4] and the GS is usually of a Fermi liquid (FL) type. However, Yb_2Pd_2Sn exhibits unconventional low-temperature properties, as it is obvious from the heat capacity $C_p(T)$ and electrical resistivity $\rho(T)$ of a polycrystalline sample shown in Fig. 1a. Plotting C_p/T vs. $\ln T$ reveals two distinct low-temperature features. First, C_p/T is very large, indicating a strongly renormalized density of states (DOS) at the Fermi energy, as expected for a Kondo system. Second, the temperature dependence of C_p/T below 2 K is logarithmic, suggesting a non-Fermi liquid (nFL) GS. These conclusions are supported by the resistivity data. The overall features of $\rho(T)$ are typical of a Kondo lattice; the maxima in $\rho(T)$ render T_K and the CEF splitting [5]. The linear resistivity ($T \leq 2$ K) is typical of a nFL. The ^{170}Yb Mössbauer data taken at 50 mK (Fig. 1b) show the absence of long range magnetic order in Yb_2Pd_2Sn. The spectrum can be explained by a purely quadrupolar hyperfine interaction; the upper limit for the Yb moment is $0.05\,\mu_B$. Thus, Yb ions in Yb_2Pd_2Sn are presumably non-magnetic, nevertheless close to a magnetic state.

The resistivity of Yb_2Pd_2Sn taken at various pressures is shown in Figs. 2(a,b). For clarity, not all pressure runs are summarised here. The low-temperature maximum observed at T_ρ^{max} for $p < 1$ GPa and $p > 4$ GPa separates the single-ion Kondo regime, where c electrons are weakly scattered on localized f states, from the coherent regime, where f and c electrons form a heavy fermion band. As discussed in Refs. 5 and 6, T_ρ^{max} scales with

T_K. In a narrow pressure-intervall, $1 \lesssim p \lesssim 4$ GPa, however, $\rho(T)$ develops new features where the maximum vanishes and a shoulder-like structure appears (see Fig. 2a). Similar anomalies occur for pressures of 1.7, 2.5 and likely at 3.5 GPa, at 0.91, 1.23 and 0.45 K respectively (Fig. 2b). Following Fisher *et al.* [7], we assume that the inflexion point of $\mathrm{d}\rho/\mathrm{d}T$ marks a magnetic phase transition. Similar features are observed in the resistivity of $Yb_2Pd_2(In, Sn)$ for concentrations at which a magnetic phase transition occurs [3]. There, the anomalies at $T = T_N$ are weak, but the antiferromagnetic (AFM) transition is clearly indicated by a sharp, λ-like, feature in the specific heat data [3]. AFM order with stable Yb-moments ($\approx 1\ \mu_B$) and a propagation vector $\vec{k} = (0, 0, 1/2)$ is revealed by elastic neutron scattering, too [8]. Such a propagation vector does not support the idea of a frustrated $S = 1/2$ XY-like spin system discussed earlier [9]. Thus, the inflexion point of $\mathrm{d}\rho/\mathrm{d}T$ likely identifies the AFM transition triggered by the pressure driven emergence of a trivalent state of the Yb ions. The enhancement of the resistivity below T_N can be understood in terms of superzone boundary effects; a gap opens in the DOS since the magnetic Brillouin zone differs from the electronic one [10]. The application of a magnetic field at $p = 2.5$ GPa (see Ref. [11]) shows that i) a field of about of 3 T quenches magnetic order, as expected for an AFM state, ii) a power law behaviour $\rho(T) \propto T^{1.6}$ develops above 3 T. Increasing the field strength to 8 T yields $\rho(T) \propto T^{1.8}$, which indicates that the field drives the system towards the FL state.

To prove magnetic order on a microscopic scale, we have carried out zero field (ZF), weak transverse field (WTF) and longitudinal field (LF) muon-spin rotation (μSR) measurements at various temperatures and pressures at the PSI μE1 beam line. μSR is a local probe measurement of the magnetic field at the muon stopping sites in the sample. If the implanted polarized muons are subject to magnetic interactions or externally applied magnetic field, their polarization $[P(t)]$ becomes time dependent. By measuring the asymmetric distribution of positrons emitted when the muons decay as a function of time, the time evolution of $P(t)$ can be deduced. Shown in Fig. 3 are ZF runs at ambient pressure (a) and $p = 1.93$ GPa (b) for various temperatures down to 0.27 K. In fact, the ZF measurements at 1.93 GPa evidence clear signs of long range magnetic order from the oscillatory behavior of the depolarization signal at lowest temperatures, vanishing for $T > T_N$, while such a feature is fully absent at ambient pressure conditions. Signatures of a Shastry-Sutherland type magnetic frustration, as proposed for $Yb_2(Pd, Ni)_2Sn$ [9], are not observed. ZF μSR measurements carried out at $T = 0.27$ K at different pressures reveal a continuous growth of the internal field, corresponding to a growth of the ordered moment, at least below 1.93 GPa. Moreover, T_N increases continuously starting from $p \gtrsim 0.7$ GPa as revealed by 50G WTF μSR data. WTF μSR experiments confirm, in addition, that magnetism is bulk by occupying more than 90% of the full sample volume, while the LF studies at $p = 1.93$ GPa suggests this magnetism to be static (at least within the muon-time window) thus corroborating the results of resistivity measurements.

The (T, p) phase diagram of Yb_2Pd_2Sn revealed by the resistivity and μSR data is sketched in the upper panel of Fig. 4. AFM order extends approximately from $p_{c1} \approx 1$ to $p_{c2} \approx 4$ GPa, while an absence of magnetic order is evident for $p < p_{c1}$ and likely for $p > p_{c2}$, at least above 100 mK. The Kondo scale inferred from the maximum of $\rho(T)$ behaves antithetic with respect to $T_N(p)$, in line with the mutually competing RKKY and Kondo coupling. The residual resistivity, $\rho_0(p)$, has a maximum in the magnetic phase and follows the shape of $T_N(p)$. Scattering of c-electrons on static imperfections yields $\rho_0 = (\hbar/e^2 l)(3\pi^2)^{1/3} n_c^{-2/3}$, where l and n_c are the mean free path and the density of the charge carriers, respectively. Usually, pressure does not modify l; thus the increase of ρ_0 reflects a decrease of n_c, in accordance with the super-zone gap-opening at the AFM transition.

The pressure dependence of T_N and T_K mimics the concentration dependence of T_N and T_K observed in $Yb_2Pd_2(In, Sn)$ [3]. For the latter, however, the Grüneisen parameter $\Omega_K = -\partial(\ln T_K)/\partial(\ln V)$ is negative for all concentrations, while in Yb_2Pd_2Sn, $\Omega_K < 0$ for $p \lesssim 2$ GPa and $\Omega_K > 0$ for $p \gtrsim 2$ GPa.

The above phase diagram can be explained by the periodic Anderson model with infinite f-f correlations, a flat c-DOS of half-width $D_0 = 2$ eV and three excited CEF doublets ($N_1 = N_2 = N_3 = 2$) separated from the ground state ($N_0 = 2$) by $\Delta_1 = 7$ meV, $\Delta_2 = 21$ meV, and $\Delta_3 = 49$ meV, respectively. The properties of the model depend on the dimensionless coupling constant $g(p)$ in an essential way. As discussed in the introduction, in Yb_2Pd_2Sn, $g(p)$ decreases at low pressures. But at large pressure which reduces the distance between the ligands, $\Gamma(p)$ and $g(p)$ increase. Thus, $g(p)$ has a minimum as a function of pressure.

At high temperatures, the model can be solved by treating the $4f$ states as incoherent Kondo scatterers [6, 12]. This yields the correlation functions as universal functions of T/T_K and also shows that the crossover between the local moment (LM) and the FL regimes takes place at T_K [13, 15]. For $n_f \simeq 1$, the coupling $g(p)$ and the scaling invariant $E_K = k_B T_K$ are related by the equation [12, 14],

$$g(p) \times \exp\left[-\frac{1}{g(p)}\right] = \left(\frac{E_K}{D}\right)^{N_0} \times \left(\frac{E_K + \Delta_1}{D + \Delta_1}\right)^{N_1} \left(\frac{E_K + \Delta_2}{D + \Delta_2}\right)^{N_2} \left(\frac{E_K + \Delta_3}{D + \Delta_3}\right)^{N_3}, \quad (1)$$

k_B is the Boltzman constant. Solving for $T_K(g)$ gives the result shown in Fig. 4(b) by the dashed line which sepa-

rates the high-entropy LM regime from the low-entropy FL one. For a given $T_K(p)$, the properties of the LM phase can be calculated by the lowest-order perturbation theory with an effective temperature-dependent coupling $g(T) \leq 1$, which is obtained by solving Eq. (1) for $D = k_B T$ [13]. The perturbative results provide a qualitative description of the experimental data and also agree with the non-crossing approximation (NCA) [6, 12] and the numerical renormalisation group calculations [13]. For $T > T_K$, we assume that the f and c states are weakly coupled and write the free energy as $F_{LM} = E_c + E_f - E_{fc} - TS_{LM}$, where E_c and E_f are the unperturbed internal energies of c and f electrons, respectively, E_{fc} is the energy gain due to the hybridization, and S_{LM} is the LM entropy reduced from the free ion value S_f by the Kondo effect. The scaling solution gives $S_{LM} = y(T)S_f$ and $E_{fc}(T) = \langle H_{cf} \rangle \simeq g(T)T_K$, where $y(T) \leq 1$; H_{cf} is the interacting part of the Hamiltonian. For $T \gg T_K$, the approximate relation $y(T) + g(T) \simeq 1$ shows that a reduction of temperatures decreases S_{LM} and increases $E_{fc}(T)$.

At low temperatures, the large entropy of Yb moments cannot be sustained and it is removed either by the screening of the LM by conduction electrons or by the onset of a long range magnetic order. For large T_K, a crossover is expected but, for small T_K, the energy gain due to the alignment of the LM leads to a magnetic GS. The energy due to the RKKY coupling is estimated by the 2nd order perturbation theory [16] which yields $E_{RKKY}(g) = zS(S+1)F(x)Dg^2$, where z is the number of nearest neighbors, S is the effective moment of Yb ions in the GS, $F(x)$ is the amplitude of the RKKY oscillations, and $x = \mathbf{r} \cdot \mathbf{k}_F$, where $\mathbf{r}$ is the distance between the LM and $\mathbf{k_F}$ is the Fermi wave vector. E_{RKKY} is calculated with unrenormalized $g(p)$, because the LM does not fluctuate in the ordered phase. Neglecting the entropy of magnetic excitations in the Néel state, we approximate the free energy as $F_N = E_c + E_f - E_{RKKY}$ and find, for $E_{RKKY} \geq E_K$, the magnetic boundary from the condition $F_N = F_{LM}$. This yields $E_{RKKY} = E_{fc} + T_N S_{LM}$ and gives $T_N(g) = k_B[T_{RKKY}(g) - g(T_N)T_K(g)]/S_{LM}$, where $T_{RKKY} = E_{RKKY}/k_B$ and $g(T_N)$ is obtained from Eq. (1) for $D = k_B T_N$. For $E_{RKKY} < E_K$, the paramagnetic entropy is removed by Kondo effect; the fully screened moments do not order magnetically.

To apply these results to Yb_2Pd_2Sn we use the CEF scheme mentioned before, take $z = 6$, $S = 3/2$, calculate $T_N(g)$ for various values of the amplitude $F(x)$, and then adjust $F(x)$ in such a way that the maximum of $T_N(g)$ coincides with the largest experimental value of $T_N(p)$. To compare theory and experiment at other pressures, we assume a linear relation between p and $g(p)$. Results are shown in Fig. 4(b), where the full line represents $T_N(g)$, and the dashed line $T_K(g)$; the unfilled symbols are for $T_N(p)$ and $T_K(p)$. The model captures the main features of the phase diagram: it describes correctly $T_K(p)$ and $T_N(p)$, and provides a reasonable explanation of the present pressure experiments.

At ambient pressure we have $E_{RKKY} < E_K$, such that the GS is non-magnetic. The NCA calculations show that $\rho(T)$ has a maximum at T_K. The application of pressure reduces E_K much faster than E_{RKKY} and leads, eventually, to $T_N > 0$. For $T_N \ll T_K$, the LMs of the ordered phase are reduced and, for $T_N \ll T \ll T_K$, the system is in the nFL state, as indicated by $\rho(T) \simeq T/T_K$. The case $T_N \leq T_K$ has to be treated with care, because the Kondo effect in the AFM phase and short-range magnetic fluctuations in the LM phase are not considered here. In that pressure range, indicated by the shaded area in Fig. 4(b), quantum critical fluctuations could reduce T_K and T_N to zero. A higher pressure yields $T_N > T_K$; but as long as T_K is close to T_N some screening of the LM remains. This implies that the AFM state, like the nFL state at a lower pressure, involves hybridized f-c states. Consequently, the AFM transition might be due to a spin density wave instability which partially gaps the Fermi surface.

As long as pressure reduces $g(p)$, the separation between T_N and T_K increases. Above some critical pressure, however, Yb ions become rigid and $\Gamma(p)$ increases. Thus, $g(p)$ saturates at first and then starts to grow. This leads to a reversed behavior of $T_N(p)$ and $T_K(p)$: the separation between T_N and T_K decreases, and the system evolves back towards the quantum critical state. Eventually, for sufficiently large pressure, we have $E_K(p) \gg E_{RKKY}(p)$ and find the FL again.

In summary, Yb_2Pd_2Sn is the first example of a heavy fermion exhibiting two pressure-driven QCPs associated with $T = 0$ magnetic instabilities. These QCPs encase a dome-like phase space with finite-temperature AFM order. The Anderson model explains the pressure dependence of T_N and T_K, and accounts for the overall behavior of $\rho(T)$ in Yb_2Pd_2Sn. We do not expect similar phase diagrams in Ce compounds, since the effective Kondo interaction and the Grüneisen parameter are monotonic functions of pressure. Thus, the electron-hole analogy between Ce and Yb materials is broken.

E.B. wishes to thank Osaka University.

[1] G.R. Stewart, *Rev. Mod. Phys.* **73**, 797 (2001); *ibid.* **78**, 743 (2006).
[2] H. v. Löhneysen *et al.*, Rev. Mod. Phys. **79**, 1015 (2007).
[3] E. Bauer *et al.*, J. Phys.: Cond. Mat. **17**, S999 (2005).
[4] E. Bauer *et al.*, Phys. Rev. B **56**, 711 (1997).
[5] D. Cox and N. Grewe, Z. Phys. B **71**, 321 (1988).
[6] V. Zlatić and R. Monnier, Phys. Rev. B **71**, 165109 (2005).
[7] M.E. Fisher and J.S. Langer, Phys. Rev. Lett. **20**, 665 (1968).
[8] E. Bauer *et al.*, Phys. Stat. Sol. B **247**, 717 (2010).
[9] F. Kikuchi *et al.*, J. Phys. Soc. Jpn. **78**, 083708 (2009).
[10] G.T. Meaden, Contemp. Phys. **12**, 313 (1971).
[11] E. Bauer *et al.*, J. Optoel. Adv. Mat. **10**, 1633 (2008).
[12] N. E. Bickers *et al.*, Phys. Rev. B **36**, 2036 (1987).
[13] A.C. Hewson, *The Kondo Problem to Heavy Fermions* (Cambridge University Press, Cambridge,1993).
[14] K. Yamada *et al.*, Prog. Theor. Phys. **71**, 450 (1984); K. Hanzawa *et al.*, J. Magn. Magn. Mat. **47-48**, 357 (1985).
[15] S. Burdin and V. Zlatić, Phys. Rev. B **79**, 115139 (2009).
[16] K. Yosida, Phys. Rev. **106**, 893 (1957)

Figures

FIG. 1: (Color online) (a) Temperature dependent specific heat Cp (left axis) and electrical resistivity ρ (right axis) of Yb_2Pd_2Sn plotted on a logarithmic temperature scale. The heat capacity is displayed as C_p/T vs. $\ln T$. The almost logarithmic dependence below 2 K is emphasized by a solid line. A core contribution $C_N \propto T^{-2}$ is subtracted from the raw data. At low temperature $\rho(T)$ is approached by a power law, $\rho(T) = \rho_0 + AT^n$, (ρ_0 is the residual resistivity, A is a material dependent constant); $n \approx 1$ implies nFl behaviour. $\rho_{100\ \mathrm{K}} \approx 91\ \mu\Omega$cm. (b) ^{170}Yb Mössbauer spectra at 50 mK of Yb_2Pd_2Sn. The solid line is a least squares fit (see text).

FIG. 2: (Color online) (a) Temperature dependent electrical resistivity, ρ, of Yb_2Pd_2Sn at various pressures, normalised to room temperature. At ambient pressure, $\rho_{\mathrm{RT}} \approx 87\ \mu\Omega$cm. Data sets are shifted by 0.05 each to improve clarity. (b) Low temperature details of $\rho(T)$ for selected pressures together with the temperature derivative -dρ/dT.The inset reveals an anomaly of $\rho(T)$ around 0.43 K at the 3.5 GPa run.

FIG. 3: (Color online) Zero field μSR spectra of Yb_2Pd_2Sn for various temperatures at 1 bar (a) and 1.93 GPa (b).

FIG. 4: (Color online) (a) Pressure-temperature phase-diagram of the magnetic ordering temperature (filled circles, resistivity; filled hexagons, μSR) and the low-temperature resistivity maximum (filled squares) of Yb_2Pd_2Sn. The filled area sketches the phase space where long range magnetic order exists. The diamonds show the pressure dependent evolution of the residual resistivity ρ_0. All lines are guides for the eye. (b) The characteristic temperatures $T_K(p)$ (dashed line), $T_{RKKY}(p)$ (short dashed line) and $T_N(p)$ (full line) of Yb_2Pd_2Sn are plotted versus the interaction strengths $g = \Gamma/\pi|E_f|$. The pressure dependence of Γ and E_f is explained in the text. Two shaded area indicate the transition region, where $T_K(p)$ and $T_N(p)$ are affected by quantum critical fluctuations. The experimental data points are added as unfilled symbols.

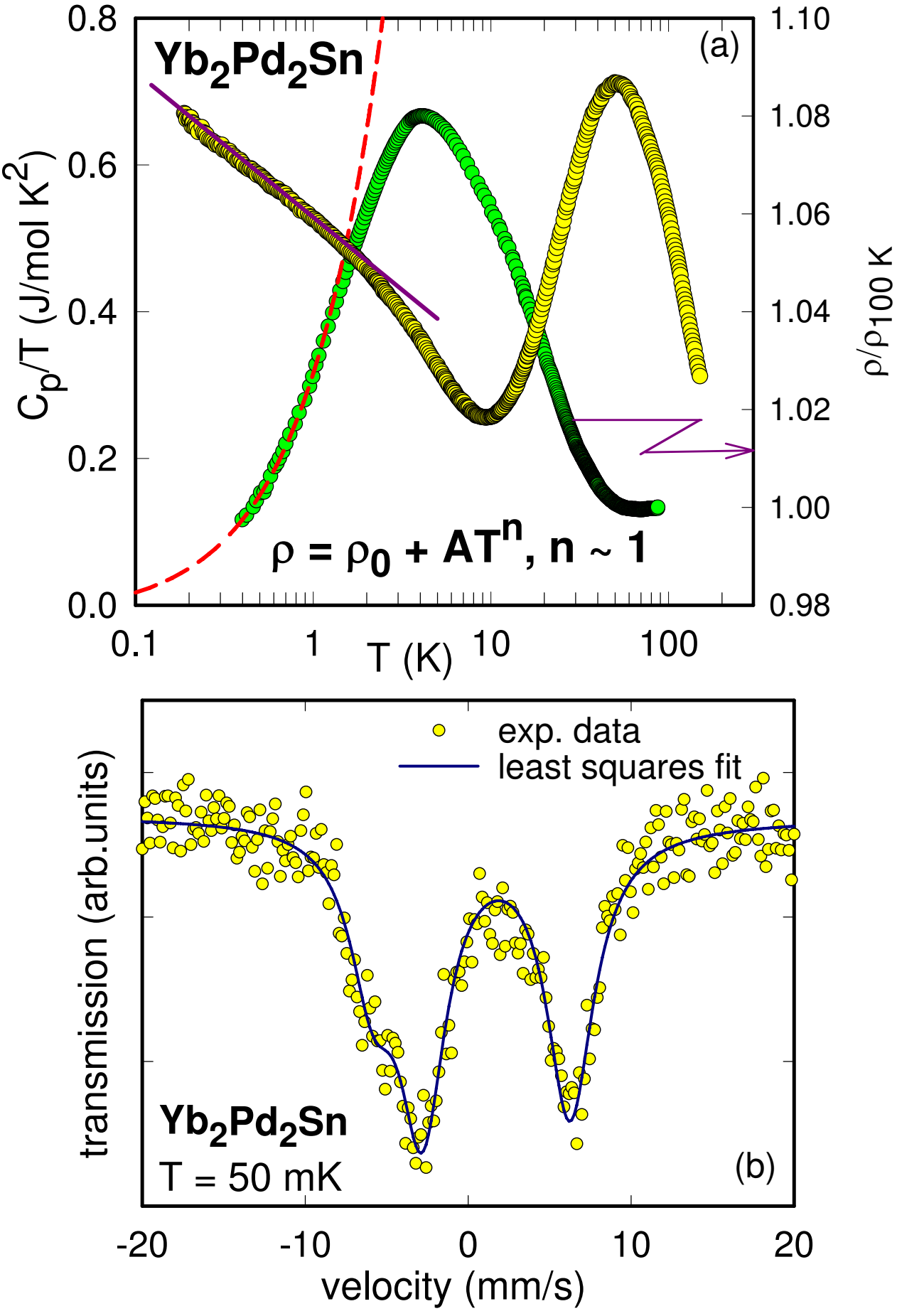

Figure 1 LH11995BR 24Mar2011

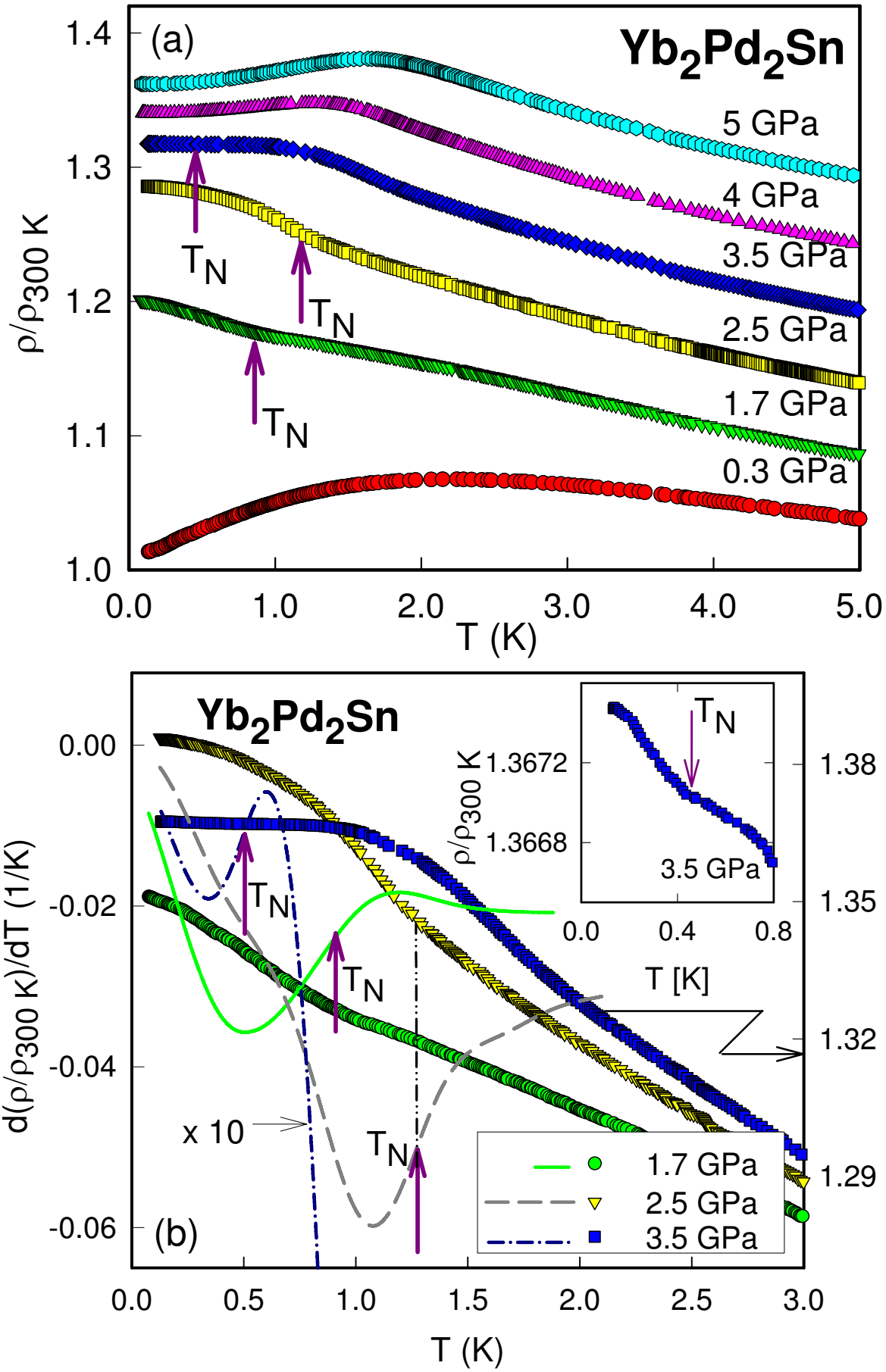

Figure 2 LH11995BR 24Mar2011

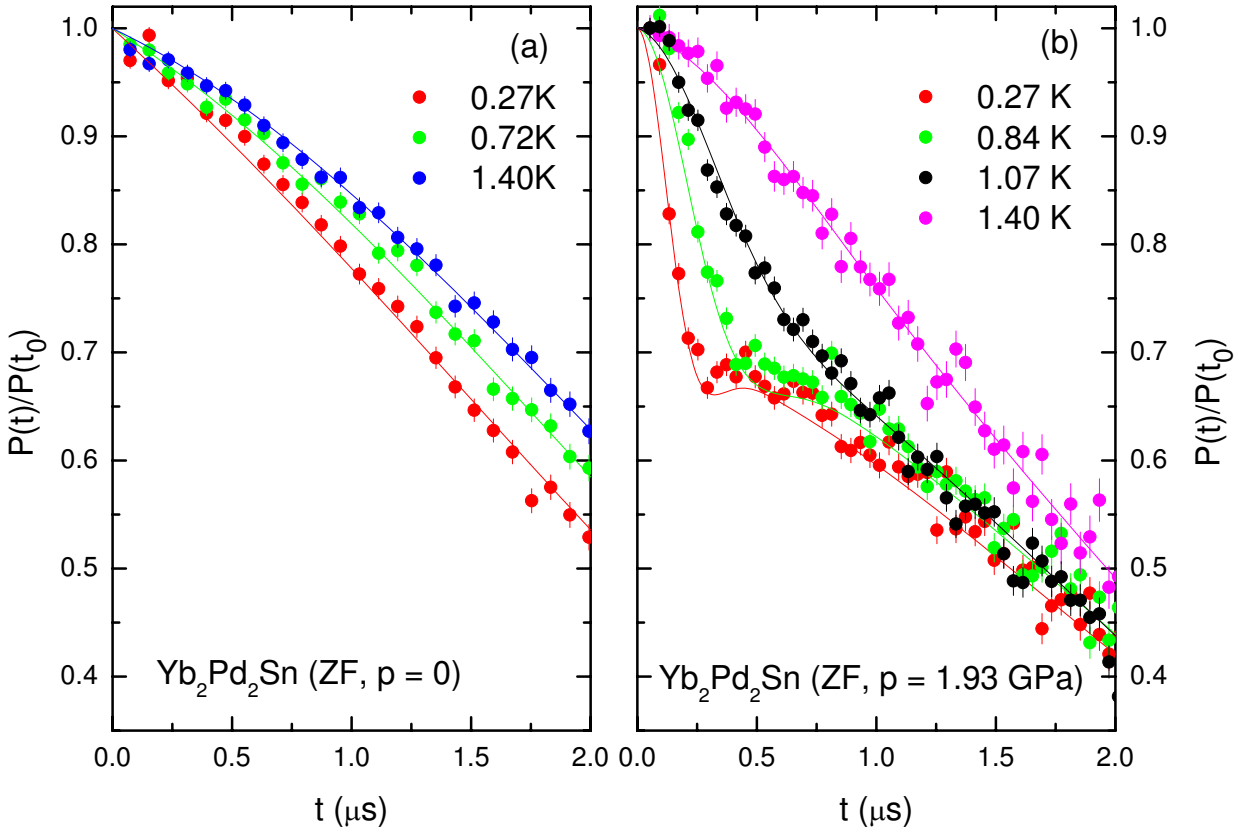

Figure 3 LH11995BR 24Mar2011

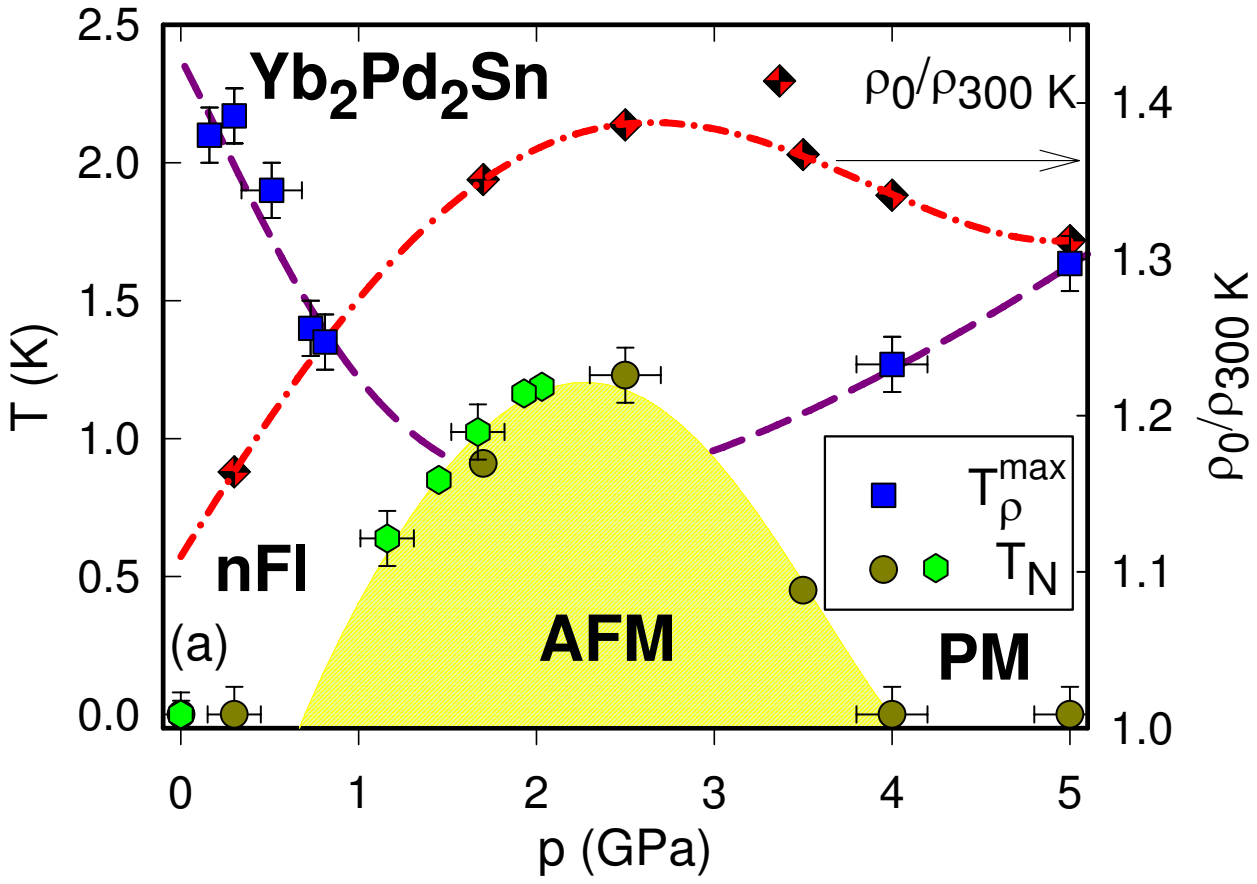

Figure 4a LH11995BR 24Mar2011

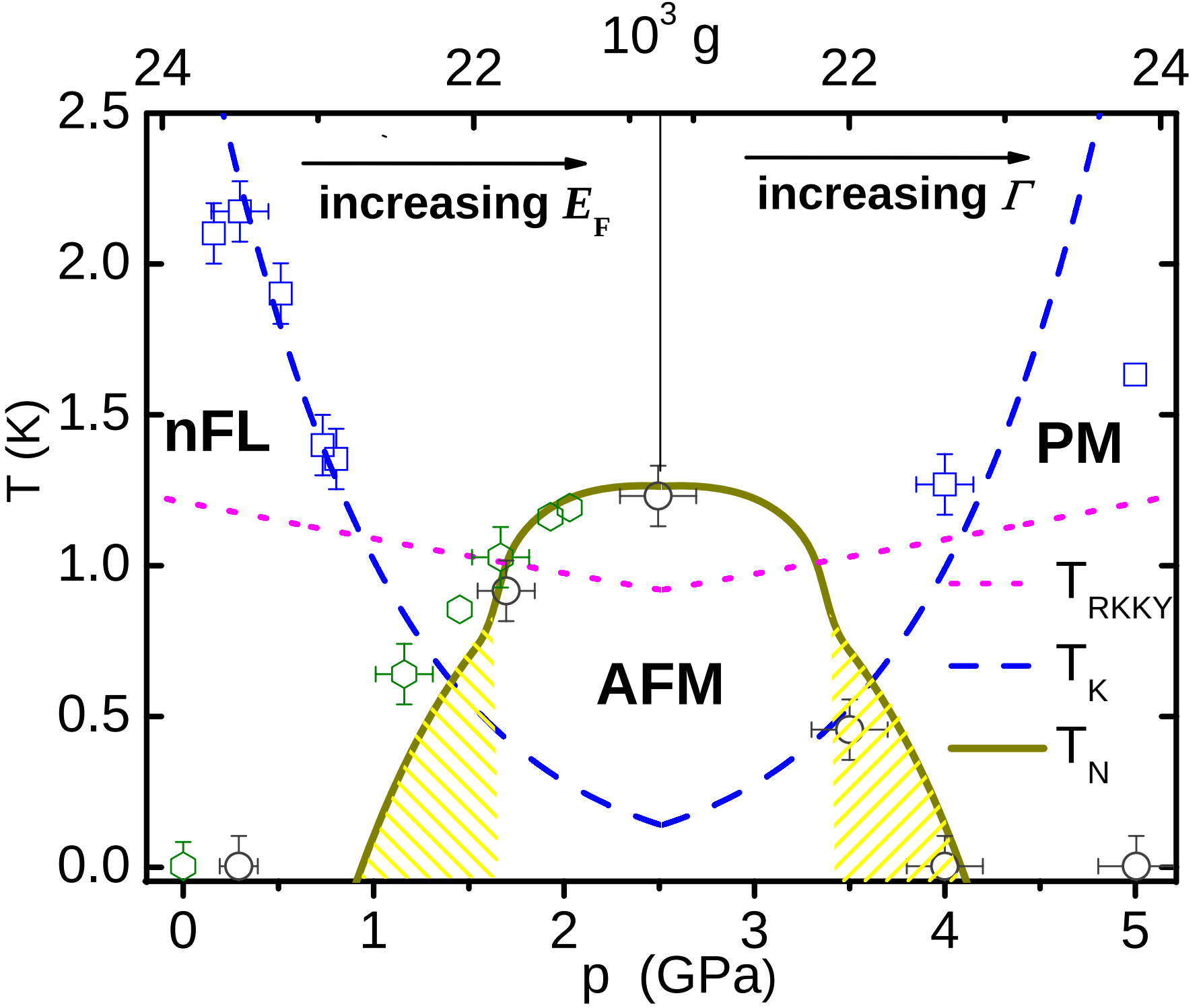
10^3 g
24
22
22
24
2.5
2.0
1.5
1.0
0.5
0.0
T (K)
increasing E_F
increasing Γ
nFL
PM
AFM
T_{RKKY}
T_K
T_N
0
1
2
3
4
5
p (GPa)